Published in final edited form as:

Cancer Discov. 2018 June ; 8(6): 750–763. doi:10.1158/2159-8290.CD-17-1368.

Chimeric Antigen Receptor T Cell-Mediated Neurotoxicity in Non-Human Primates

Agne Taraseviciute[1,2,3], **Victor Tkachev**[1,2,3], **Rafael Ponce**[4], **Cameron J. Turtle**[2], **Jessica M. Snyder**[5], **H. Denny Liggitt**[5], **David Myerson**[2,6], **Luis Gonzalez-Cuyar**[6], **Audrey Baldessari**[7], **Chris English**[7], **Alison Yu**[1], **Hengqi Zheng**[1,3], **Scott N. Furlan**[1,2,3], **Daniel J. Hunt**[1], **Virginia Hoglund**[1], **Olivia Finney**[1], **Hannah Brakke**[1], **Bruce R. Blazar**[8], **Carolina Berger**[2], **Stanley R Riddell**[2], **Rebecca Gardner**[1], **Leslie S. Kean**[1,2,3,*], and **Michael C. Jensen**[1,2,3,*]

[1]The Ben Towne Center for Childhood Cancer Research, Seattle Children's Research Institute, Seattle WA

[2]The Fred Hutchinson Cancer Research Center, Seattle WA

[3]Department of Pediatrics, University of Washington, Seattle WA

[4]Juno Therapeutics, Seattle WA

[5]Deparment of Comparative Medicine, University of Washington, Seattle WA

[6]Department of Pathology, University of Washington, Seattle WA

[7]Washington National Primate Research Center, University of Washington, Seattle, WA

[8]Department of Pediatrics, University of Minnesota, Minneapolis MN

Abstract

Chimeric Antigen Receptor (CAR) T cell immunotherapy has revolutionised the treatment of refractory leukemias and lymphomas, but is associated with significant toxicities, namely cytokine release syndrome (CRS) and neurotoxicity. A major barrier to developing therapeutics to prevent CAR T cell-mediated neurotoxicity is the lack of clinically relevant models. Accordingly, we developed a rhesus macaque (RM) model of neurotoxicity via adoptive transfer of autologous CD20-specific CAR T cells. Following cyclophosphamide lymphodepletion, CD20 CAR T cells expand to 272–4450 cells/μl after 7–8 days and elicit CRS and neurotoxicity. Toxicities are associated with elevated serum IL-6, IL-8, IL-1RA, MIG and I-TAC levels, and disproportionately high cerebrospinal fluid (CSF) IL-6, IL-2, GM-CSF and VEGF levels. During neurotoxicity, both CD20 CAR and non-CAR T cells accumulate in the CSF and in the brain parenchyma. This RM model demonstrates that CAR T cell-mediated neurotoxicity is associated with pro-inflammatory CSF cytokines and a pan-T cell encephalitis.

[*]**Corresponding Authors:** Leslie S. Kean, Ben Towne Center for Childhood Cancer Research, 1100 Olive Way, Suite 100, Seattle WA 98101 Phone: (206)884-4079 Fax: (206)884-4100 Leslie.kean@seattlechildrens.org, Michael C. Jensen, Ben Towne Center for Childhood Cancer Research, 1100 Olive Way, Suite 100, Seattle WA 98101 Phone: (206)884-7300 Fax: (206)884-4100 michael.jensen@seattlechildrens.org.

[*]Dual Senior Authors

Conflict of interest disclosure statement: No potential conflicts of interest were disclosed by the other authors.

Keywords

CAR T cell immunotherapy; Neurotoxicity; Cytokine Release Syndrome; Non-Human Primate; Animal Model

INTRODUCTION

CD19-specific CAR T cell immunotherapy can mediate the regression of relapsed and refractory leukemias and lymphomas (1–4). However, the side effects and toxicities of this therapy, particularly in acute lymphoblastic leukemia (ALL) patients with high tumor burden, are significant and can be life-threatening (5–7). The most common toxicities include cytokine release syndrome (CRS) and neurotoxicity, which have resulted in a number of patient deaths in multiple CAR T cell trials (5–11). The neurologic toxicities span a wide spectrum, ranging from transient word-finding difficulties, visual and auditory hallucinations, delirium and movement disorders, to encephalopathy and seizures. Rapid onset cerebral edema, unresponsive to medical measures, is a rare but lethal event reported in numerous clinical trials (12). Corticosteroids and the anti-IL6 receptor (IL-6R) monoclonal antibody (tocilizumab) can ameliorate CRS; however, medical interventions to reduce the incidence and severity of neurotoxicity are currently lacking (7,10,11).

At present, the pathobiology of severe neurotoxicity associated with CAR T cell activation and expansion has not been defined and animal models are needed to derive mechanistic insights and test therapeutic interventions. To address these limitations, we have developed the first non-human primate (NHP) model of CRS and neurotoxicity, using CD20 CAR T cells in RMs. This model recapitulates the key aspects of CAR T cell on-target effects such as CAR T cell expansion with induction of B cell aplasia as well as CRS and neurotoxicity, and clarifies that toxicities are neither 1) tumor-dependent, 2) specific CAR T cell-dependent, nor 3) CD19 antigen-specific. Moreover, it demonstrates that neurotoxicity is associated with a complex program of immune activation that results in asymmetrically high levels of pro-inflammatory cytokines and chemokines in the CSF and widespread infiltration of the brain parenchyma with both, EGFRt+ (CD20 CAR) and EGFRt− (non-CAR) T cells in equal proportions to those present in the circulation.

RESULTS

χHIV and SIV lentiviral transduction of RM T cells

RMs express multiple tripartite motif-containing 5α (TRIM5α) isoforms that confer resistance to retroviral infection, resulting in poor transduction efficiency with HIV-1-based lentiviruses due to HIV-1 capsid degradation (13). In order to overcome this restriction, and to improve transduction efficiency, we utilized two previously developed lentiviruses, χHIV (HIV-1-based vector genome packaged with an SIV capsid), and SIV (SIV vector genome packaged with an SIV capsid) for RM T cell transductions (14,15). The CD20 CAR χHIV or SIV lentivirus vectors housed a huEF1p or a CAG promoter, respectively, a human/RM cross-reactive CD20-specific second generation 4-1BB:zeta CAR, a T2A ribosomal skip sequence, and a truncated human EGFR marker (Supplementary Fig. S1A) (16,17).

Following anti-CD3/anti-CD28 bead activation, immunomagnetically purified RM T cells were amenable to transduction with GFP-χHIV (R.301), GFP-χHIV and CD20CAR/EGFRt-χHIV (R.302), CD20CAR/EGFRt-χHIV (R.301, R.303) and CD20CAR/EGFRt-SIV (R.304) lentiviruses, at multiplicity of infections (MOIs) ranging from 1 to 5, resulting in transduction efficiencies of 22–75% (Fig. 1A)

Ex vivo expansion, composition and cytolytic activity of RM CD20 CAR T cells

Following transduction, CD20 CAR T cell products were successfully expanded for all recipients (R.301–R.304, $n = 4$) by addition of IL-2 (50 U/ml) to X-vivo 15 cell culture medium to achieve the targeted cell dose of 1×10^7 CD20 CAR T cells/kg. *Ex vivo* T cell expansion ranged from 5 to 36-fold after 8 to 17 days of culture (Supplementary Table S1). The final GFP+ and EGFRt+ (CD20 CAR) T cell products at the end of *ex vivo* culture were used for adoptive transfer experiments and consisted of a ~2:1 CD8:CD4 ratio (60.6 +/− 1.7%: 28.4 +/− 3.6%; $n = 5$) (Fig. 1A). We further assessed the CD20 CAR T cell products with respect to the relative proportions of CD28+/CD95+ (NHP central memory phenotype), CD28−/CD95+ (NHP effector memory phenotype) and CD28+/CD95− (NHP naïve phenotype) T cells in both, EGFRt+ (CD20 CAR) and EGFRt− (non-CAR) populations at the end of *ex vivo* expansion (Fig. 1B). In the four CD20 CAR T cell products, the majority of EGFRt+ T cells displayed a CD28+/CD95+, central memory phenotype, for both CD4 (85 +/− 8.4%) and CD8 cells (67.6 +/− 8.1%) (Fig. 1B, top). Similarly, the majority of EGFRt− T cells also displayed a CD28+/CD95+ phenotype, for both CD4 (78.5 +/− 9%) and CD8 cells (56.7 +/− 7.5%) (Fig. 1B, bottom). A smaller proportion of EGFRt+ T cells displayed a CD28−/CD95+ effector memory phenotype, for both CD4 (12.7 +/− 8.2%) and CD8 cells (29.2 +/− 8.7%), while very few cells displayed a CD28+/CD95− naïve phenotype, for both CD4 (1 +/− 0.8%) and CD8 cells (1 +/− 0.5%) (Fig. 1B, top). The same phenotype was observed in the EGFRt− T cells in the products (CD28−/CD95+ CD4: 18.1 +/− 9.6% CD4 and CD8: 41.9 +/− 8.2% cells; CD28+/CD95− CD4: 1.9 +/− 1.4% and CD8: 0.8 +/− 0.5% cells) (Fig. 1B, bottom). These data demonstrate that the majority of T cells in the infused products comprised a CD28+/CD95+, or central memory phenotype, a T cell subset that has been shown to mediate enhanced T cell activity in murine models, and increased persistence following adoptive transfer in NHP studies (18,19). Furthermore, although the infused cell products contained both EGFRt+ (CD20 CAR) and EGFRt− (non-CAR) T cells, their CD4 and CD8 T cell phenotypes were similar irrespective of CD20 CAR expression. We subsequently monitored these T cell phenotypes longitudinally *in vivo* following CD20 CAR T cell adoptive transfer.

We assessed the *in vitro* cytolytic activity of each of the CD20 CAR-transduced T cell products in a chromium release assay by their ability to mediate CD20-specific cytolysis of both human (CD20-K562) and RM (RM B-LCL) cells with a wide range of CD20 antigen expression (Fig. 1C). CD20-specific cytotoxicity was demonstrated by the lack of CD20 CAR T cell-mediated cytolysis of human K562 cells, which do not express CD20 (Fig. 1C).

In vivo expansion and B cell aplasia following adoptive transfer of autologous RM CD20 CAR T cells

The schema used for adoptive transfer of CD20 CAR T cells into RMs is outlined in Fig. 2A. For the first recipient, R.301, 48 days prior to the CD20 CAR T cell infusion, we administered autologous GFP T cells, following lymphodepletion, to assess the impact of adoptive transfer of T cells lacking the CD20 CAR construct. The GFP T cell infusion was well tolerated, without any observed clinical toxicities (Fig. 3A, B and Fig. 4A, R.301 GFP). As expected, GFP T cells failed to undergo expansion (peak level of 28 GFP+ T cells/μl) and did not induce B cell aplasia (Fig. 2B, R.301 GFP). These cells were not measurable in the peripheral blood after Day 14 post-infusion (Fig. 2B, R.301 GFP). These findings were similar to a previous report of CAR T cells targeting the solid tumor antigen ROR1 in RM, which demonstrated limited expansion and persistence of ROR1 CAR T cells (20). In contrast, upon transfer of CD20 CAR T cells to all four recipients, R.301–R.304, the CD20 CAR T cells underwent significant expansion, with peak levels of 272 to 4450 (mean level 1987 +/− 987) EGFRt+ T cells/μl in the peripheral blood, which occurred on day 7 to 8 post-infusion (Fig. 2B). This EGFRt+ T cell expansion was accompanied by a concomitant B cell aplasia in all four recipients, which occurred on day 5 to 7 following CD20 CAR T cell infusion (Fig. 2B). Thus, the CD20 antigen load prior to lymphodepletion was 700 +/− 394 cells/μl, and after lymphodepletion, but prior to CAR T cell infusion, 135 +/− 32 cells/μl in blood, and these cells became unmeasurable concomitant with CAR T cell expansion. In two recipients that were followed long term, R.301 and R.302, B cell aplasia persisted through day 32 (R.301) and day 43 (R.302) (Fig. 2B).

In two pilot experiments R.301 and R.302 were also evaluated for the impact of an infusion of T cells engineered to express the CD20 antigen (RhCD20 T-APC) on CD20-CAR T cell expansion and persistence. A single infusion of RhCD20 T-APCs on day 47 had no effect on CD20 CAR T cell numbers in R.301, likely due to the fact that the T-APCs were administered when the CD20 CAR T cells were no longer detectable and native B cells had reconstituted in the peripheral blood (Fig. 2B). In contrast, a single infusion of RhCD20 T-APCs administered on day 15 after CD20 CAR T cell transfer in R.302, resulted in a 10-fold increase in circulating EGFRt+ T cell numbers, from 9 to 93 EGFRt+ cells/μl, measured 5 days following T-APC administration. These data suggest that engineered RhCD20 T-APCs are potentially capable of activating and expanding circulating CD20 CAR T cells and represents an important area for future investigations.

CAR and non-CAR T cell dynamics following adoptive CD20 CAR T cell transfer

Following adoptive transfer of CD20 CAR T cells, activation and expansion of both EGFRt+ (CD20 CAR) and, to a lesser extent, EGFRt− (non-CAR) T cell populations was observed (Fig. 2B,E and Supplementary Fig. S2). This expansion favored CD8 T cells, which resulted in an increased CD8:CD4 EGFRt+ ratio of 9.1 +/− 2 in all four recipients (R.301–R.304) during peak expansion following CD20 CAR T cell infusion, compared to a ratio of 2.2 +/− 0.3 in the starting infused products ($P = 0.03$, Fig. 2D). Although R.303 displayed a more modest increase in the CD8:CD4 EGFRt+ ratio compared to other recipients, in this recipient we observed a significant expansion of CD8+CD4+ double-positive EGFRt+ T cells (previously shown to represent an effector population in RMs (21)), which were not

captured in the CD8:CD4 ratio. While EGFRt− (non-CAR) T cells, also underwent proliferation (Fig. 2E, top two panels), their CD8:CD4 ratio during peak expansion was minimally skewed to CD8 T cells, 1.6 +/− 0.8, which was significantly different from the CD8:CD4 ratio of EGFRt+ T cells at the same time point ($P = 0.01$), yet unchanged from the day 0 (pre-CD20 CAR T cell infusion) CD8:CD4 EGFRt− ratio of 0.6 +/− 0.05 ($P = 0.2$, Fig. 2D). In addition to enumerating the expansion of EGFRt+ (Fig. 2B) and EGFRt− T cells (Supplementary Fig. S2), we also measured their proliferation status by Ki-67 expression (Fig. 2E). Both EGFRt+ CD4 and CD8 cells were highly proliferative, with Ki-67 levels reaching 89.8 +/− 4.9% in CD4 and 94 +/− 4.4% in CD8 cells in all four recipients (R.301–R.304) during peak expansion, which approximated the proliferation in EGFRt+ cells in the starting infused products: 84 +/− 5% in CD4 and 90.3 +/− 4.4% CD8 cells. Although both CD4 and CD8 EGFRt− (non-CAR) cells also increased concomitantly with CD20 CAR T cell expansion, their level of proliferation was significantly less compared to EGFRt+ cells, with Ki-67 expression of 38.5 +/− 7% in CD4 and 51.5 +/− 13% in CD8 cells ($P = 0.02$ for CD4, $P = 0.02$ for CD8; Fig. 2E, top two panels). The EGFRt+ cells displayed a trend toward higher levels of CD25 in comparison to EGFRt− cells, suggesting that they were more activated during proliferation, however this difference in CD25 expression was not statistically significant (77.3 +/− 12% vs 45.8 +/− 18% for CD4 ($P = 0.09$) and 77.8% +/− 13% vs 47.8% +/− 17% for CD8 ($P = 0.15$)) (Fig. 2E). In addition to proliferation and activation, we also monitored the longitudinal dynamics of memory, effector and naive T cell phenotypes of CD20 CAR T cells after adoptive transfer. Within both CD4 and CD8 EGFRt+ (CD20 CAR) T cells, we observed the preservation of a similar proportion of the CD28+/CD95+, central memory subset during peak expansion compared to infused product (78.3 +/− 6.2% vs 85 +/− 8.4% for CD4 ($P = 0.5$) and 61.9 +/− 8.6% vs 67.6 +/− 8.1% for CD8 ($P = 0.2$)). The same was true for the CD28−/CD95+, effector memory subset (15.5 +/− 6.6% vs 12.7 +/− 8.2% for CD4 ($P = 0.8$) and 24.8 +/− 10% vs 29.2 +/− 8.7% for CD8 ($P = 0.7$)), and CD28+/CD95−, naïve subset (3.6 +/− 2.8% versus 1 +/− 0.77% CD4 ($P = 0.5$) and 8.3 +/− 7.7% versus 1 +/− 0.5% CD8 ($P = 0.4$)) when EGFRt+ T cell subsets were compared at peak expansion to infused product (Fig. 2F). This data suggests that the majority of EGFRt+ (CD20 CAR) T cells maintain a CD28+/CD95+, central memory phenotype *in vivo*, during peak expansion, at similar proportions to those present in the infused CD20 CAR T cell products. It should be noted that differences that were observed in the proportion of EGFRt+ CD28+/CD95+ CD8 cells in R.301 and R.302, after T-APC infusion (Fig. 2F) may have been affected by the T-APC infusion, and thus conclusions about the natural history of CAR T cell phenotypes in these animals cannot be made.

Clinical and laboratory manifestations of cytokine release syndrome (CRS) following CD20 CAR T cell transfer

After adoptive cell transfer, we closely monitored the clinical status of each recipient for specific signs and symptoms of CRS and neurotoxicity. All of the recipients of CD20 CAR T cell infusions developed clinical signs of CRS and exhibited abnormal neurologic manifestations (described in detail below), which was in contrast to R.301 after the control GFP T cell infusion. Weight loss exceeding 10% occurred in two of four animals, R.301 and R.302, while temperature instability, characterized by fever (>101F), occurred in all four

animals (R.301–R.304), and hypothermia (<98F) occurred in one animal (R.301), after CD20 CAR T cell infusion (Fig. 3A, right). CRP was elevated to peak levels of 2.8 to 4.2-fold above the upper limit of normal (ULN) in all recipients of CD20 CAR T cells and accompanied CAR T cell expansion, but remained within normal limits in R.301 following non-CAR, GFP T cell infusion (Fig. 3B). Ferritin and LDH levels were more heterogeneous: in two recipients, R.301 and R.302, peak ferritin was elevated 2.1 and 4.2-fold above the ULN (180 ng/ml), while peak LDH was elevated 6.7 and 9.6-fold above the ULN (210 U/L), respectively, following CD20 CAR T cell infusion (Fig. 3B). In the remaining two recipients, R.303 and R.304, we observed normal ferritin levels and modestly elevated peak LDH levels (2.1 and 1.3-fold above ULN, respectively) following CD20 CAR T cell infusion (Fig. 3B). To examine changes in cytokine levels following CD20 CAR infusion, we serially measured the serum levels of 29 NHP cytokines and chemokines. We found that levels of pro-inflammatory cytokines IL-6, IL-8, IL-1RA and chemokines, MIG (CXCL9) and I-TAC (CXCL11) were statistically significantly elevated in all four recipients (R.301–R.304) following CD20 CAR T cell infusion compared to pre-infusion levels (Fig. 3C). In CD20 CAR T cell recipients, the peak serum levels of IL-6 were elevated 12-fold, to 14.7 +/− 3.5 pg/ml ($P = 0.008$), IL-8 levels were elevated 3.3-fold, to 127.8 +/− 26 pg/ml ($P = 0.02$), IL-1RA levels were elevated 10-fold, to 2694.3 +/− 633 pg/ml ($P = 0.009$), MIG levels were elevated 79-fold, to 1268.7 +/− 457.9 pg/ml ($P = 0.03$) and I-TAC levels were elevated 23-fold, to 2151 +/− 448.2 pg/ml ($P = 0.004$), compared to pre-infusion levels (peak levels were observed on days 2–10 following CAR T cell infusion, pre-infusion levels were measured on day −7 or day −8 prior to infusion; Fig. 3C. The full panel of cytokines measured is shown in Supplementary Fig. S3).

Neurotoxicity following CD20 CAR T cell transfer

To quantify the neurologic impact of CD20 CAR T cell therapy, we developed a clinical scoring system for neurotoxicity (described in Methods and Supplementary Table S2). Neurotoxicity occurred in all recipients receiving CD20 CAR T cells (R.301–R.304, $n = 4$), with the most severe neurotoxicity observed between days 7–14 following infusion (Fig. 4A). The most common neurotoxicity symptoms included tremor (ranging from minimal to severe), decreased activity or lethargy, slow movements and ataxic gait (Fig. 4A and Supplementary Table S2). Tremors and decreased activity level as well as lethargy contributed the most to the neurotoxicity score, while slow movement, ataxia and seizures had a smaller contribution to the total score (Fig. 4A). These neurologic symptoms have also been reported in some patients following CD19 CAR T cell therapy, where tremors, decreased level of consciousness and ataxia/other abnormal movements were reported in 19%, 25% and 10% of patients with neurologic toxicity, respectively (12). Three of the four recipients (R.301–R.303) were treated with Levetiracetam (15 mg/kg BID or TID), which was started after neurologic symptoms manifested. Levetiracetam therapy was maintained for 8–11 days following full resolution of all neurologic symptoms (through day 22 for R. 301 and day 29 for R.302) or until study end point (day 12 for R.303) (Fig. 4A arrows). R. 304 underwent a planned terminal analysis on day 8 after CD20 CAR T cell infusion, prior to the start of Levetiracetam. For R.301 and R.302, who were followed long term, neurotoxicity symptoms waned and resolved at 14 and 18 days after CD20 CAR T cell infusion, respectively, concurrent with CD20 CAR T cell contraction (Fig. 4A).

Clinical neurotoxicity with accumulation of both EGFRt+ (CD20 CAR) and EGFRt− (non-CAR) T cells and pro-inflammatory cytokines in the cerebral spinal fluid (CSF)

Given that in human clinical trials of CD19 CAR T cell therapy, high numbers of CD19 CAR T cells were found in the CSF and correlated with neurotoxicity (22), we sought to determine whether CD20 CAR T cells also accumulated in the CSF in the RM model. In three recipients (R.302–R.304), the CSF was examined longitudinally and revealed trafficking of T cells into the CSF after adoptive CD20 CAR T cell transfer, coincident with CAR T cell expansion in the blood and the onset of clinical neurotoxicity (Fig. 4B and Supplementary Fig. S4B). Importantly, the T cell accumulation in the CSF included *both* EGFRt+ (CD20 CAR) and EGFRt− (non-CAR) cells, with the proportion of each closely mirroring that in the peripheral blood (Fig. 4B). Notably, when cytokine levels were measured in the CSF and compared to time-matched levels in the serum, these were markedly different for several cytokines, demonstrating increased concentrations of multiple pro-inflammatory cytokines in the CSF relative to serum (Fig. 4C). This included increased concentrations of IL-6 (478-fold increase, mean peak CSF level 5314.7 +/− 175 pg/ml, mean serum level 11.1 +/− 3.2 pg/ml, $P = 0.000007$), IL-2 10-fold increase, mean peak CSF level 118 +/− 21.1 pg/ml, mean serum level 11.9 +/− 11.9 pg/ml, $P = 0.012$), GM-CSF (8.2-fold increase, mean peak CSF level 1.96 +/− 0.09 pg/ml, mean serum level 0.24 +/− 0.16 pg/ml, $P = 0.00077$) and VEGF (6.3-fold increase, mean peak CSF level 6.95 +/− 1.8 pg/ml, mean serum level 1.1+/− 0.26 pg/ml, $P = 0.03$; Fig. 4C). IL-1β, IL-1RA, MCP-1 and IP-10 levels were also asymmetrically elevated in the CSF, however the difference between CSF and serum did not reach statistical significance. IL-1β was elevated 7.8-fold (mean peak CSF level 25.4 +/− 13.4 pg/ml, mean serum level 3.27 +/− 0.5 pg/ml, $P = 0.17$), IL-1RA was elevated 6.3-fold (mean peak CSF level 13338 +/− 7048.6 pg/ml, mean serum level 2129 +/− 1273 pg/ml, $P = 0.19$), MCP-1 was elevated 13.7-fold (mean peak CSF level 3405 +/− 1603.7 pg/ml, mean serum level 248 +/− 81.1 pg/ml, $P = 0.12$) and IP-10 was elevated 97-fold (mean peak CSF level 849 +/− 439.8 pg/ml, mean serum level 8.7 +/− 7.8 pg/ml, $P = 0.13$) in the CSF compared to paired serum samples (Fig. 4C, the full panel of serum cytokines is included in Supplementary Fig. S3 and CSF cytokines in Supplementary Fig. S5).

Symptomatic neurotoxicity is associated with pan-encephalitis of large numbers of activated EGFRt+ (CD20 CAR) and EGFRt− (non-CAR) T cells

To date, limited data are available as to the numbers, composition, and activation state of T cells within the brain parenchyma of human subjects experiencing CAR T cell neurotoxicity. To rigorously determine the anatomic correlates of neurotoxicity and trafficking of EGFRt+ (CD20 CAR) and EGFRt− (non-CAR) T cells to the CNS, we performed timed necropsies on recipients R.303 (on day 12, during peak neurotoxicity symptoms which included moderate tremors and lethargy, slow movements and ataxia (with ataxia manifested by an animal's inability to maintain balance on a perch and/or the need for support to maintain balance while sitting or standing) and R.304 (on day 8, during peak CD20 CAR T cell expansion, at the onset of neurotoxicity symptoms which included mild tremor and decreased activity on day 7), in order to assess the degree of CSF and brain infiltration at pre-determined times after T cell infusion. We focused on specific regions of the brain, including the frontal, parietal, temporal and occipital lobes, cerebellum, hippocampus, basal

ganglia, brainstem, choroid plexus, meninges and thalamus. These experiments demonstrated that, for R.304, during peak CAR T cell expansion (on day 8 after CD20 CAR T cell transfer), histopathologic changes were present in all regions of the brain examined, including in both, the gray and white matter, and were exemplified by mild multifocal meningitis and mild to moderate, multifocal perivascular T cell cuffing, as demonstrated by H&E staining in the basal ganglia and the parietal lobe (Fig. 5A, bottom panels). In R.303, the recipient that underwent planned terminal analysis during peak neurotoxicity (on day 12 after CD20 CAR T cell transfer), minimal histopathologic cerebral abnormalities were demonstrated on H&E staining, with most of the brain appearing normal. However, rare abnormalities were observed in R.303, as demonstrated by focal perivascular edema and focal perivascular inflammation (Fig. 5A, top panels). Although there was marked histopathologic heterogeneity observed in H&E brain sections from R.303 and R.304, immunofluorescence analysis for CD3-expressing T cells in the brain demonstrated a pattern of wide-spread intra-parenchymal cellular infiltration in both animals, which was observed in all the brain regions analysed, including the frontal lobe, parietal lobe, occipital lobe, temporal lobe, cerebellum, and thalamus. Despite differences in brain histopathology in R. 303 and R.304, we did not observe any consistent variation in cytokine or biochemical markers of CRS or neurologic symptoms that were predictive of these differences.

T cell infiltration into the brain parenchyma, without predilection for specific brain regions, revealed increased CD3 cell infiltration in the cerebellum, parietal lobe and thalamus in R. 304 (day 8 post-CAR T infusion) compared to R.303 (day 12 post-CAR T infusion) and compared to normal RM brain (Fig. 5B). Notably, the perivascular T cell infiltration observed in R.304 was analogous to key histopathologic changes in the brain of an adult patient who developed severe CRS and neurotoxicity, characterized by delirium that progressed to coma, who died 13 days following CD19 CAR T cell infusion secondary to cerebral edema (Fig. 5C) (12). T cell infiltration of the brain did not appear to be antigen dependent, given the lack of CD20 expression in normal RM brain (Supplementary Fig. S5A) as measured by immunofluorescence. Moreover, we found that brain T cell infiltration was comprised of both EGFRt+ (CD20 CAR) and EGFRt− (non-CAR) T cells, in similar proportions to those observed in the CSF and in the blood (Fig. 5D). Thus, on day 8 after adoptive transfer of CD20 CAR T cells in R.304, when 80.5% of CD3 cells were EGFRt+ in the blood, and 97% in the CSF, the brain also contained a similar proportion, 90.2% EGFRt+ T cells (Fig. 5D). Likewise, when analysed on day 12 after CD20 CAR T cell transfer in R. 303, following CD20 CAR T cell contraction, there was a predominance of EGFRt− (non-CAR) T cells, with only 3% of CD3 cells remaining that were EGFRt+ in the blood, 3.7% in the CSF, and 5.9% EGFRt+ T cells in the brain (Fig. 5D). The CD8:CD4 T cell balance was also interrogated in the brains of R.303 and R.304 and compared to the CD8:CD4 balance in the blood and in the CSF. In R.304, there was a predominance of CD8 EGFRt+ T cell infiltration in the brain (94%) which was closely mirrored the blood (92%) and CSF (93%), on day 8. R.303 also showed a predominance of CD8 EGFRt+ T cells in the brain (84%), which was slightly higher than the balance in the CSF (72%) and significantly higher than the CD8:CD4 balance observed in the blood (59%). The EGFRt− (non-CAR) T cells infiltrating in the brain were also more highly skewed toward CD8 EGFRt− T cells

compared to the peripheral blood in both R.303 (brain (90%), CSF (73%) and blood (45%)) and R.304 (brain (88%), CSF (71%) and blood (39%)) (Fig. 5D).

We further examined the phenotypic characteristics of EGFRt+ and EGFRt− T cells in the CSF (R.302–R.304 (n = 3)) and the brain (R.304 (n = 1)) during peak expansion compared to T cells in the blood (normal controls (n=5), prior to CAR T cell infusion (d0) or at peak CAR T cell expansion (days −7–8) (R.301–R.304 (n = 4)). We measured T cell proliferation (by Ki67 expression) and activation (by CD25 and CD69 expression). Both CD4 and CD8 EGFRt+ T cells were highly proliferative in the blood when compared to CD4 and CD8 EGFRt− (non-CAR) T cells on days 7–8 (CD4: 91.5 +/− 2% vs 20.1 +/− 2%, P = 0.003; CD8: 92.5 +/− 2.7% vs 40.9 +/− 9.6%, P = 0.01; Fig. 5E) or compared to day 0 or to normal controls (CD4: 24.8 +/− 5%, CD8: 10.4 /− 1.3%, day 0; CD4:14.5 +/− 3.8%, CD8: 2.8 +/− 0.4%, normal controls; Fig. 5E). Substantial levels of Ki67 expression were observed in both, CD4 and CD8 EGFRt+ (CD20 CAR) and EGFRt− (non-CAR) T cells in the CSF (CD4: 73.3 +/− 1.5% and 45.3 +/− 12.9% respectively, P = 0.07; CD8: 84.4 +/− 3% and 70.8 +/− 6.4 respectively, P = 0.19; (Fig. 5E). Although CD25 expression could be measured on both EGFRt+ and EGFRt− CD4 and CD8 T cells in the blood, CSF and brain following CD20 CAR T cell infusion, no significant differences in CD25 expression levels were observed when compared to day 0 pre-infusion and normal control blood samples (Fig. 5E). Similarly, although CD69 expression could be measured in both CD4 and CD8 EGFRt+ and EGFRt− T cells in the blood, CSF and brain compartments following CD20 CAR T cell infusion (CD4: 51.7 +/− 8.5%, 66.7 +/− 13.2%, 97.6% vs 18.6 +/− 3.4%, 47.1 +/− 17.5%, 93.5% EGFRt+ vs EGFRt−; CD8: 52.8 +/− 7.6%, 66.9 +/− 20.2%, 96.3% vs 34.7 +/− 0.9%, 54.7 +/− 17.2% and 95.8% EGFRt+ vs EGFRt−) these were not significantly different from CD69 levels in the blood on day 0 or in normal controls (CD4: 26.5 +/− 8.1%, 26.5 +/− 5.2%; CD8: 34.6 +/− 5.7%, 41.7 +/− 3.3%; Fig. 5E).

We also examined one of the key integrins involved in T cell migration through the blood brain barrier, the α4β1 integrin (also known as ‘VLA-4’), which mediates T cell adhesion to cerebral endothelial cells through interaction with VCAM-1 (23). We examined changes in α4 and β1 integrin expression in EGFRt+ (CD20 CAR) and EGFRt− (non-CAR) T cells to determine if there were any associations between integrin expression and CAR-T expansion and the observed infiltration of these cells into the CNS (Supplementary Fig. S5C). As expected, α4β1 integrin was expressed in CD4 and CD8 T cells in the blood of normal control RMs (CD4: 49.2 +/− 3.6%, CD8: 78.5 +/− 3.6%) and in the blood of R.301–R.304 on day 0, prior to CAR T infusion (CD4: 48.9 +/− 8.4%, CD8: 41.3 +/− 8.1%; Supplementary Fig. S5C). During peak CD20 CAR T cell expansion, α4β1 integrin levels were significantly increased in the blood in both CD4 and CD8 EGFRt+ T cells compared to EGFRt− T cells (CD4: 67.3 +/− 3.1% vs 42.9 +/− 9.8%, P = 0.00004; CD8: 78.8 +/− 2.6% vs 47.4 +/− 2%, P = 0.03; Fig. S5C). For CD8+ EGFRt+ cells, this expression level was similar to that found in normal controls. For CD4+ EGFRt+ cells this represented an increase compared to normal controls (P = 0.0009; Fig S5C). While preliminary, this data suggests that upregulation of integrins may facilitate trafficking of T cells into the brain after CAR-T infusion.

DISCUSSION

CAR T cells represent a breakthrough therapy, capable of inducing remission in patients with relapsed or refractory B-cell ALL, NHL and CLL, many of whom have failed all other available therapies (1–4). However, this therapy has also been associated with significant toxicities, including severe CRS and fatal neurotoxicity, the cause of which has not yet been determined (5–7). Here, we describe the first NHP model of CAR T cell targeting of B cells that also recapitulates CRS and neurotoxicity.

This model has identified two major components of CAR T cell-mediated neurotoxicity that point to a complex interplay between soluble factors and cell-mediated processes: (1) the selective increase of multiple pro-inflammatory cytokines in the CSF compared to serum during peak CD20 CAR T cell expansion and (2) the concurrent development of encephalitis, in which both CAR and non-CAR T cells accumulate in the CSF and the brain. These observations point to a program of cytokine release following CAR T cell activation, resulting in systemic and CSF inflammation, disruption of the blood brain barrier and subsequent CAR and non-CAR T cell infiltration of the CSF and CNS.

The pathobiology of CAR T cell-associated neurotoxicity remains obscure and is limited by the availability of CSF and tissue samples from patients participating in CAR T cell trials. However, the hypothesis that neurotoxicity in patients is caused by a unique effector mechanisms elicited by CD19CAR-specific CAR T cells in response to CD19 antigen in the brain, (24) based on either tumor seeding or physiologic CD19 expression within the CNS, appears to be less likely based on the following observations from this study: (1) CD20 CAR T cells caused neurotoxicity in the absence of identifiable CD20 expression in the normal RM brain, or occult B cell tumor cells in the CNS; and (2) both CAR and non-CAR T cells infiltrate the brain. These observations, in addition to lack of neurotoxicity reported in antibody therapies targeting CD20 (Rituximab, Ofatumumab and Obinutuzumab) (25) are more consistent with an antigen-independent encephalitis during neurotoxicity resulting from CAR and non-CAR T cell activation outside the CNS. However, although we demonstrated that normal RM brain lacks CD20 expression via immunofluorescence (Supplementary Fig. S4A), it is possible that more sensitive, molecular approaches may be able to detect this antigen in the brain. This possibility is supported by the recently described CNS lymphatic system (26), and the data from the NIH Blueprint NHP Atlas using molecular probes for CD20 (MS4A1 transcript) (http://www.blueprintnhpatlas.org) (27). The role that antigen-specificity and/or antigen load plays in neurotoxicity therefore remain open questions, and critical areas for future studies.

We demonstrated a disproportionate increase in pro-inflammatory cytokine and chemokine levels in the CSF compared to serum, during neurotoxicity following CD20 CAR T cell infusion, which provides clues as to the mechanism underlying neurotoxicity. First, it points to the possibility of selective cytokine accumulation in the CSF, either due to increased influx, from the blood to the CSF, or due to decreased efflux, from the CSF into the blood. Indeed, in studies of systemic inflammation, increased cytokine influx of TNFα and decreased efflux of prostaglandin E_2 have been identified as key mechanisms that result in cytokine retention in the CSF. Alternatively, or in addition, it suggests that high levels of

CSF cytokines could represent cytokine production *in situ*, either by T cells that have trafficked to the brain or by resident CNS cells, such as microglia, astrocytes or activated endothelial cells (12,28,29). In experimental autoimmune encephalitis (EAE), an animal model for neuroinflammation in multiple sclerosis, activated microglia produce pro-inflammatory cytokines including IFNγ, TNFα and IL-1β as well as the chemokine MCP-1 (29). In patients with relapsing remitting MS, CSF levels of IFNγ have been found to be elevated (30). Furthermore, CSF levels of IL-6, IL-8, IP-10, RANTES, MCP-1 and MIG were also elevated in patients with neuropsychiatric systemic lupus erythematosus (SLE), an inflammatory autoimmune disorder that includes symptoms such as headaches, mood disorders, seizure and psychosis (31). A more recent study of adult patients with neurotoxicity following CD19 CAR T cell therapy has identified endothelial activation and vascular disruption as key features associated with neurotoxicity, and highlighted the important role of brain vascular pericytes, which produce IL-6 and VEGF in response to IFNγ (12). The extent to which these different mechanisms drive neurotoxicity await further investigation in the NHP model, with the ultimate goal of identifying pharmacologically targetable pathways in order to ameliorate this toxicity.

The complexity of the inflammatory response and neurotoxicity that occurs with CD19 and CD20 CAR T cells is unusual compared to other cellular adoptive therapies, including donor lymphocyte infusions as well as CAR T cells directed at other antigens, such as the non-mature B cell, solid tumor antigen, ROR1 (20). However, given the fact that no post-mortem examination of the brain was performed in either the previous ROR1 CAR experiments (20) or in the GFP control experiment described here, it remains possible that sub-clinical CNS abnormalities could occur. As such, further detailed studies of the CNS after infusion of CAR T cells that do not cause overt neurotoxicity would be beneficial to the field. Nevertheless, there is precedence in the literature for neurotoxicity with other immune agonists (including IL-2, IFNα, the CD3–CD19 bi-specific T cell engager Blinatumomab, as well as the CD28 agonist TGN1412), each of which have been associated with a similarly complex spectrum of neurologic abnormalities (32–34). As with CAR T cells, the precise mechanistic pathways leading to the perturbation of CNS homeostasis with these agents has yet to be fully dissected. While the pathways are still undetermined, there is also a commonality of each of these immune activation syndromes with what has been termed ‘Sepsis-associated encephalopathy’ or ‘septic encephalopathy’, in which cerebral dysfunction, characterized by delirium or coma, occurs in the setting of sepsis in the absence of direct cerebral infection (35). While multiple upstream inciting factors exist, the common final pathway involves a significant breach of the integrity of the blood-brain-barrier (BBB) neurovascular unit, as well as astrocyte dysfunction (36). This BBB breach is clearly evident in RM recipients of CD20 CAR T cells, given the accumulation of both cytokines and T cells in the CNS in these animals. The extent to which systemic cytokine release ignites the breakdown of the BBB is at this point unclear, but there is commonality in the cytokines upregulated during sepsis and those during CAR T cell mediated CRS (prominently including IL-1β, IL-6, IL-8 and others), suggesting that finding and neutralizing the common cellular source of these cytokines, rather than targeting individual molecules, could be more successful in preventing the breach of the BBB and resultant neurotoxicity (35).

Our data (and that from patients) also provides a potential explanation for the ineffectiveness of currently available therapies, such IL-6R blockade with Tocilizumab, to ameliorate neurotoxicity. Treatment with Tocilizumab has been shown to improve signs of CRS (reduction in fever and hypotension), however it has not been shown to prevent or improve neurotoxicity. With our novel NHP model, we now have the opportunity to test alternative strategies to ameliorate neurotoxicity, which include 1) blocking CAR and non-CAR T cell infiltration into the CNS by the use of natalizumab, an anti-α4 integrin antibody used clinically in MS patients to block leukocyte infiltration into the CNS, 2) modulating cytokine production by T cells through CAR engineering approaches or 3) depleting the source of CNS cytokine production by targeting activated endothelial cells or microglia.

In summary, the experiments presented here describe the first NHP model of CAR T cell-mediated CRS and neurotoxicity. They point to a complex program of systemic and local neuroinflammation leading to this clinical complication, which includes the accumulation of pro-inflammatory cytokines in the CSF and significant expansion and activation of both CAR and non-CAR T cells as well as their migration into the CSF and brain parenchyma. This model represents a platform for detailed interrogation into the mechanisms driving neurotoxicity after adoptive cellular therapy and for pre-clinical testing of therapeutic strategies to eliminate this deadly complication of adoptive immunotherapy.

METHODS

GFP, RhCD20 and CD20 CAR vectors and lentivirus production

GFP-χHIV lentivirus was generated using a SIN-HIV-1-based lentiviral vector expressing enhanced GFP-firefly luciferase (EGFP-ffluc), under the control of the human elongation factor 1 alpha promoter, huEF1p. RhCD20-χHIV lentivirus was generated using a codon-optimized Rhesus CD20 (RhCD20) sequence synthesized by Genewiz (Genewiz, USA), based on the coding region of the predicted cDNA sequence of rhesus macaque CD20 (RefSeq: XM_001086364.1), and insertion, following NheI/NotI restriction enzyme digestion, into a SIN-HIV-1-based lentiviral vector, under the control of the huEF1p. The second generation 4-1BB:zeta CD20CAR construct encoded a Leu16 (murine anti-human CD20) single chain variable fragment (scFv) fused to a human IgG4 C_H2-C_H3 hinge, including two mutations in the C_H2 region (L235D and N297Q, both of which reduce binding to FcγR) (37), a CD28 transmembrane domain, a 4-1BB (CD137) co-stimulatory domain and CD3ζ domain. The CD20CAR-4-1BB:zeta construct also contained a transduction and selection marker downstream of a *Thoseaasigna* virus 2A (T2A) peptide sequence, comprising a truncated epidermal growth factor receptor (EGFRt) domain (Supplementary Fig. S1) (16,17). This expression cassette was incorporated into either a SIN-HIV-1- or a SIV-based lentiviral vector, under the control of the huEF1p or the CMV early enhancer/chicken beta actin (CAG) promoter, respectively, and used to generated either χHIV- or SIV-based lentiviruses (14,15). GFP, RhCD20 or CD20 CAR-expressing χHIV lentiviruses were generated by four plasmid (the χHIV Gag/Pol plasmid, HIV-1 Rev/Tat plasmid, VSV-G envelope plasmid, and either GFP, RhCD20 or CD20 CAR-expressing SIN-HIV-1-vector plasmid) co-transfection of 293T cells (ATCC), using Lipofectamine 2000 (Invitrogen). The CD20 CAR-expressing SIV lentivirus was similarly generated by four

plasmid (the SIV Gag/Pol plasmid, SIV Rev/Tat plasmid, VSV-G envelope plasmid, and the CD20 CAR-expressing SIV-vector plasmid) co-transfections of 293T cells, using Lipofectamine 2000. Lentivirus-containing supernatant was collected 72–96 hours after transfection and concentrated by ultracentrifugation at 24,500 rpm for 1 hour 34 minutes at 4°C and the virus was titered using human H9 T cells (ATCC).

Transduction and expansion of rhesus macaque (RM) T cells

PBMCs were isolated from adult RM peripheral blood by standard protocols, using Ficoll-Paque PLUS (GE Healthcare Bio-Sciences). Total T cells were isolated from PBMCs using a NHP pan T cell isolation kit per manufacturer‘s instructions (Miltenyi Biotec; Supplementary Table S3). Polyclonal T cells were activated with NHP anti-CD2/anti-CD3/anti-CD28 stimulation beads at a 1:2 bead to T cell ratio (Miltenyi Biotec) in X-vivo 15 medium (Lonza) supplemented with 10% fetal bovine serum (FBS) (HyClone), 1% penicillin/streptomycin/L-glutamine (Invitrogen), 50 μM beta-mercaptoethanol (Sigma) and recombinant human IL-2 (rhIL-2, 50 U/mL; R&D Systems). Lentiviral transduction with spinoculation was performed on day 2 or 3 using polybrene (8 μg/ml; Sigma) and χHIV-GFP, χHIV-RhCD20, χHIV- or SIV-CD20 CAR lentiviruses (MOI range: 1–5). Stimulation beads were removed between day 6 and 8 of culture. T cell cultures were supplemented with IL-2 (50 U/ml) three times per week. At the end of the stimulation cycle, after 8–17 days of culture, T cells were washed in 1× PBS and infused as fresh cells, for R.301, or cryopreserved into cell bank aliquots, for R.302–R.304, and subsequently thawed, washed in 1× PBS and resuspended in 1× PBS supplemented with 10% autologous plasma immediately prior to infusion. These culture conditions yielded a final product with a ~2:1 ratio of CD8:CD4 T cells (Fig. 1A). In this study, we did not select a 1:1 C8:CD4 GFP+ or EGFRt+ T cell ratio for infusion, as the RM experiments were designed to parallel the original CD19 CAR T cell clinical trial at our institution that did not use a defined CD8:CD4 T cell ratio (ClinicalTrials.gov #NCT01683279).

Cell lines

The human K562 chronic myelogenous leukemia (CML) cell line was obtained from the European Collection of Cell Cultures through Sigma-Aldrich in 2012. K562 cells were authenticated by STR profiling matched to DSMZ database by the University of Arizona Genetics Core on 10/12/2015. Dr. Amitinder Kaur produced the RM B-Lymphoblastoid Cell Lines (B-LCLs), Mm211.98 (B-LCL1) and Mm309.98 (B-LCL2), by herpesvirus transformation of allogeneic RM B cells, acquired in 2014 (38). B-LCLs were not authenticated. The CD19-transgene and CD20-transgene expressing-K562 cell lines (CD19-K562 and CD20-K562) were previously described and obtained from Stanley Riddell in 2012 (39). CD19-K562 and CD20-K562 were not authenticated. K562, CD19-K562 and CD20-K562 cell lines were cultured in RPMI (Invitrogen) supplemented with 10% FBS (HyClone) and 1% L-glutamine (Invitrogen). B-LCL1 and B-LCL2 cell lines were cultured in RPMI supplemented with 20% FBS and 1% Penicillin/Streptomycin/L-glutamine (Invitrogen). All cell lines were negative for *Mycoplasma* using qPCR-based testing (Sigma Lookout mycoplasma kit or Promokine PCR mycoplasma kit). All cell lines used in these experiments were between passage 1 and 18.

Chromium release RM CD20 CAR T cell cytotoxicity assay

Human target cells, K562, CD19-K562 and CD20-K562, and RM target cells, B-LCL1 and B-LCL2, were labeled with ^{51}Cr (Perkin Elmer), washed and incubated in triplicate in 96-well round-bottom plates with human or RM effector T cells (Mock, CD19 CAR- and CD20 CAR-transduced T cells) at various effector to target (E:T) ratios. Supernatants were collected after a 4-hour incubation for γ-counting using Top Count NTX (Perkin Elmer), and percent specific lysis was calculated as previously described (40).

Immunophenotypic analysis of RM GFP or CD20 CAR T cell products

Immunophenotyping was performed using fluorophore-conjugated mAbs: CD3, CD4, CD8, CD19, CD20, CD25, CD28, CD29, CD49d, CD95 and Ki-67 (Supplementary Table S3). Cell surface expression of EGFRt was detected using APC-conjugated anti-EGFR mAb, cetuximab (Supplementary Table S3). CD28 and CD95 antibodies were used to assess T cell phenotypes (central memory, effector memory, and naïve) in the products and longitudinally *in vivo* (41). Flow cytometric analysis was performed on the LSRFortessa (BD Biosciences), and data was analysed using FlowJo software (Treestar).

RM *in vivo* adoptive T cell transfer studies

NHP experiments were performed according to the Guide for the Care and Use of Laboratory Animals of the National Institutes of Health, which were approved by the University of Washington Institutional Animal Care and Use Committee (IACUC). Each recipient received Cyclophosphamide (Baxter) as lymphodepleting chemotherapy. R.301 received 30 mg/kg cyclophosphamide/dose administered on 2 consecutive days, starting on day −7 prior to GFP-expressing control cell infusion. Because R.301 tolerated the cyclophosphamide infusion well, and to optimize lymphodepletion and dose-similarity to clinical practice,, all subsequent CD20 CAR T cell infusions were performed after 2 doses of 40 mg/kg/dose cyclophosphamide. R.301 received Cyclophosphamide on day −6 and day −5 prior to CAR T cell infusion. R.302 and R.304 received Cyclophosphamide on day −7 and day −6 prior to CAR T cell infusion. R.303 received Cyclophosphamide on day −4 and day −3 (Cyclophosphamide lymphodepletion was delayed by 3 days in R.303 due to pulmonary complications in the recipient on day −7, following central catheter placement, necessitating clinical observation prior to being deemed eligible to safely proceed by the veterinarian on day −4) prior to CAR T cell infusion. Mesna (Sagent Pharmaceutical) was administered to each recipient as a bladder protectant. The total Mesna dose was equal to the Cyclophosphamide dose (30–40 mg/kg/day), divided into 4 doses (7.5–10 mg/kg/dose), administered intravenously (IV), 30 minutes prior, and 3, 6 and 8 hours after Cyclophosphamide infusion. GFP control (R.301 only), a combination of GFP and CD20 CAR T cells (1:1 ratio, R.302 only) or CD20 CAR T cells (R.303 and R.304) were infused, intravenously (IV), at doses ranging from 0.6 to 1.2×10^7 GFP+ or EGFRt+ T cells/kg. All recipients received antibiotic prophylaxis with Ceftazidime and Vancomycin, antiviral prophylaxis with Acyclovir and antifungal prophylaxis with Fluconazole, additional antibiotics included Enrofloxazin, administered to R.301–R.303 during neutropenia at the discretion of the veterinarian. Recipients underwent clinical and neurologic monitoring

according to the scoring system in Supplementary Table S2. In addition, blood, lymph nodes and bone marrow aspirates were collected longitudinally in all recipients.

Evaluation of GFP T cell or CD20 CAR T cell engraftment, anti-CD20 effector function and integrin expression following adoptive transfer

CD20 CAR T cell engraftment was monitored longitudinally via flow cytometry by detection of EGFRt+ T cells in peripheral blood, bone marrow, and lymph node specimens. The accumulation of both EGFRt+ (CD20 CAR) and EGFRt− (non-CAR) T cells was also tracked longitudinally in the CSF and in brain specimens obtained at necropsy. For flow cytometric analysis, the cells were prepared as follows: peripheral blood erythrocytes in whole blood (WB), PBMC, and bone marrow samples were lysed using BD Pharm Lyse solution (BD Biosciences). Following lysis, Fc block was performed (for all CD20 CAR T cell recipients) in 1× PBS containing 20% autologous RM plasma. Cell surface epitopes were stained with directly labeled antibodies in Fc block followed by Cytofix/Cytoperm fixation and permeabilization (BD Biosciences) and intracellular staining with directly labeled antibodies. Lymph nodes were dissociated through wire mesh and collected cells were washed in 1× PBS prior to antibody incubation. CSF collections were performed via lumbar or foramen magnum puncture, CSF supernatant was processed for cytokine analysis and CSF cells were collected via centrifugation for flow cytometric evaluation.

Measurement of laboratory markers of cytokine release syndrome (CRS) after GFP or CD20 CAR T cell transfer

Blood samples were collected longitudinally before and after CD20 CAR T cell infusion and analysed at the University of Washington clinical laboratory for C-reactive protein (CRP), Ferritin and lactate dehydrogenase (LDH).

Measurement of clinical neurotoxicity after CD20 CAR T cell transfer

A neurologic monitoring strategy was developed which allowed us to assess the animal’s activity level, movement speed, presence of tremors, gait abnormalities, and seizure, before and after CD20 CAR T cell transfer (Supplementary Table S2). This resulted in a calculated Neurotoxicity Score. Recipients were scored for their neurologic symptoms, twice daily using the scoring system and raw scores were reported (Supplementary Table S2).

Histopathologic analysis, immunohistochemical (IHC) and immunofluorescence (IF) staining of RM brain sections

Board certified veterinary pathologists (J.M.S, A.B. and H.D.L) analysed neuropathologic features in hematoxylin and eosin (H&E)-stained brain sections, and images were acquired using the NIS-Elements Basic Research v3.2 for 64-bit imaging software (Nikon Instruments) and plated in Adobe Photoshop Elements (Adobe Systems). Image brightness and contrast were adjusted using auto white balance and/or auto contrast corrections that were applied to the entire image.

For CD3 and CD20 IHC peroxidase staining, slides containing brain sections embedded in paraffin, were baked and deparaffinized on the Leica Bond Automated Immunostainer (Leica Biosystems). Antigen retrieval was performed using Citrate, followed by blocking

with normal goat serum (10% in TBS). Slides were incubated with primary antibodies, CD3 (Clone LN10, 1:250 dilution; Leica Biosystems), CD20 (Clone L26, 1:500 dilution; Leica Biosystems) or mouse IgG control, in Leica Primary Antibody Diluent. The Leica Bond Post Primary was used followed by Leica Bond Polymer. For substrate detection, slides were incubated with the Leica Bond Mixed Refine (DAB) substrate detection kit, followed by Hematoxylin (Leica Biosystems) counterstain. Sections were cleared to Xylene and mounted with synthetic resin mounting medium and cover slips.

For IF staining, paraffin sections were placed on silanized slides and slides were deparaffinised in Citrisolv (Thermo Fisher Scientific), followed by 100% ethanol to water. Heat-induced antigen retrieval was performed by placing slides into a decloaking chamber (Biocare Medical). Universal blocking was performed using Background Sniper (Biocare Medical). Slides were incubated with anti-CD3 (Bio-Rad) and anti-smooth muscle actin (SMA) antibodies and washed in 1× PBS (Gibco). Secondary antibody incubation was performed with goat anti-rat AF 488 and goat anti-mouse IgG2a AF568 (Invitrogen), and slides were washed in 1× PBS followed by water. Hoechst dye (Invitrogen) was used for nuclear counter stain. Slides were mounted using ProLong antifade gold + DAPI mounting medium (Invitrogen) and images captured using the Nuance microscope (Perkin Elmer).

RM cytokine measurements in the serum and CSF

Serum and CSF supernatant samples were stored at −80°C prior to cytokine analysis. Samples were thawed and clarified by centrifugation (16,000 × g at 4°C). Undiluted samples were incubated with Monkey Cytokine Magnetic 29-Plex antibody beads (Invitrogen). For analyte detection, the Biotinylated Detector Antibody was used followed by Streptavidin-RPE, per manufacturer's instructions. Levels of cytokines and chemokines were measured using the Bioplex-200 system (Bio-Rad).

Brain dissociation, T cell purification and flow cytometry

RM brains were harvested at necropsy after perfusion with 3 to 5 L of room temperature 1× PBS until organ pallor and clear fluid was visually confirmed at the perfusion exit site. A veterinary pathologist (A.B) identified and sectioned multiple sections of the brain (frontal lobe, parietal lobe, temporal lobe, occipital lobe, cerebellum, hippocampus, basal ganglia, brainstem, choroid plexus, meninges and thalamus). The brain tissue was enzymatically dissociated using the human tumor dissociation kit (Miltenyi Biotec), washed with 1× PBS and passed through a 70μm strainer. Debris removal solution (Miltenyi Biotec)was used followed by immunophenotypic analysis on isolated cells using flow cytometry as described above.

Statistical analysis

Unless otherwise indicated, data are expressed as means +/− s.e.m. Differences between values were examined using the parametric two-tailed unpaired Student's *t*-test, and differences were considered to be significant when $P < 0.05$.

Supplementary Material

Refer to Web version on PubMed Central for supplementary material.

Acknowledgments

Financial support (including the source and number of grants, for each author): This work was supported by the US National Institutes of Health (grant P01CA065493 (to B.R.B.), 1R01HL095791, 2U19AI051731, 1UM1AI126617, U19AI117945, R33AI116184 (to L.S.K.) and 2R01CA136551 (to M.C.J)) and the Fred Hutchinson Cancer Research Center/University of Washington Cancer Consortium Cancer Center Support grant (to M.C.J.). A.T. was supported by a departmental Ruth L. Kirschstein NRSA training grant (T32CA009351). Additional support to A.T. was provided by the St. Baldrick's Fellowship, ASCO Conquer Cancer Young Investigator Award and ASBMT New Investigator Award.

M.C. Jensen reports receiving a commercial research grant from Juno Therapeutics, has ownership interest (including patents) in Juno Therapeutics, and is a consultant/advisory board member for Juno Therapeutics. L.S. Kean reports receiving a commercial research grant from Juno Therapeutics. S.R. Riddell reports receiving a commercial research grant from Juno Therapeutics, has ownership interest (including patents) in Juno Therapeutics, and is a consultant/advisory board member for Adaptive Biotechnology, Cell Medica, Juno Therapeutics, and Omniox. C.J. Turtle reports receiving a commercial research grant from Juno Therapeutics, has a patent application shared with Fred Hutchinson Cancer Research Center, and is a consultant/advisory board member for Adaptive Biotechnologies, Bluebird Bio, Celgene, Gilead, Juno Therapeutics, Precision Biosciences, and Seattle Genetics.

References

1. Park JH, Geyer MB, Brentjens RJ. CD19-targeted CAR T-cell therapeutics for hematologic malignancies: interpreting clinical outcomes to date. Blood. 2016; 127:3312–20. [PubMed: 27207800]
2. Maude SL, Teachey DT, Porter DL, Grupp SA. CD19-targeted chimeric antigen receptor T-cell therapy for acute lymphoblastic leukemia. Blood. 2015; 125:4017–23. [PubMed: 25999455]
3. Tasian SK, Gardner RA. CD19-redirected chimeric antigen receptor-modified T cells: a promising immunotherapy for children and adults with B-cell acute lymphoblastic leukemia (ALL). Ther Adv Hematol. 2015; 6:228–41. [PubMed: 26425336]
4. Gardner RA, Finney O, Annesley C, Brakke H, Summers C, Leger K, et al. Intent-to-treat leukemia remission by CD19 CAR T cells of defined formulation and dose in children and young adults. Blood. 2017; 129:3322–31. [PubMed: 28408462]
5. Lee DW, Gardner R, Porter DL, Louis CU, Ahmed N, Jensen M, et al. Current concepts in the diagnosis and management of cytokine release syndrome. Blood. 2014; 124:188–95. [PubMed: 24876563]
6. Maude SL, Frey N, Shaw Pa, Aplenc R, Barrett DM, Bunin NJ, et al. Chimeric Antigen Receptor T Cells for Sustained Remissions in Leukemia. New England Journal of Medicine. 2014; 371:1507–17. [PubMed: 25317870]
7. Hay KA, Hanafi L-A, Li D, Gust J, Liles WC, Wurfel MM, et al. Kinetics and biomarkers of severe cytokine release syndrome after CD19 chimeric antigen receptor-modified T-cell therapy. Blood. 2017; 130:2295–306. [PubMed: 28924019]
8. Davila ML, Riviere I, Wang X, Bartido S, Park J, Curran K, et al. Efficacy and Toxicity Management of 19–28z CAR T Cell Therapy in B Cell Acute Lymphoblastic Leukemia. Science Translational Medicine. 2014; 6:224ra25.
9. Maude SL, Barrett D, Teachey DT, Grupp SA. Managing cytokine release syndrome associated with novel T cell-engaging therapies. Cancer J. 2014; 20:119–22. [PubMed: 24667956]
10. Bonifant CL, Jackson HJ, Brentjens RJ, Curran KJ. Toxicity and management in CAR T-cell therapy. Molecular Therapy — Oncolytics. 2016; 3:16011. [PubMed: 27626062]
11. Brudno JN, Kochenderfer JN. Toxicities of chimeric antigen receptor T cells: recognition and management. Blood. 2016; 127:3321–30. [PubMed: 27207799]

12. Gust J, Hay KA, Hanafi L-A, Li D, Myerson D, Gonzalez-Cuyar LF, et al. Endothelial Activation and Blood-Brain Barrier Disruption in Neurotoxicity after Adoptive Immunotherapy with CD19 CAR-T Cells. Cancer Discov. 2017; 7:1404–19. [PubMed: 29025771]
13. Evans ME, Kumkhaek C, Hsieh MM, Donahue RE, Tisdale JF, Uchida N. TRIM5α variations influence transduction efficiency with lentiviral vectors in both human and rhesus CD34(+) cells in vitro and in vivo. Molecular therapy : the journal of the American Society of Gene Therapy. 2014; 22:348–58. [PubMed: 24153115]
14. Uchida N, Hargrove PW, Lap CJ, Evans ME, Phang O, Bonifacino AC, et al. High-efficiency transduction of rhesus hematopoietic repopulating cells by a modified HIV1-based lentiviral vector. Molecular therapy : the journal of the American Society of Gene Therapy. 2012; 20:1882–92. [PubMed: 22871664]
15. Hanawa H, Hematti P, Keyvanfar K, Metzger ME, Krouse A, Donahue RE, et al. Efficient gene transfer into rhesus repopulating hematopoietic stem cells using a simian immunodeficiency virus-based lentiviral vector system. Blood. 2004; 103:4062–9. [PubMed: 14976042]
16. Jonnalagadda M, Mardiros A, Urak R, Wang X, Hoffman LJ, Bernanke A, et al. Chimeric antigen receptors with mutated IgG4 Fc spacer avoid fc receptor binding and improve T cell persistence and antitumor efficacy. Mol Ther. 2015; 23:757–68. [PubMed: 25366031]
17. Wang X, Chang W-C, Wong CW, Colcher D, Sherman M, Ostberg JR, et al. A transgene-encoded cell surface polypeptide for selection, in vivo tracking, and ablation of engineered cells. Blood. 2011; 118:1255–63. [PubMed: 21653320]
18. Sommermeyer D, Hudecek M, Kosasih PL, Gogishvili T, Maloney DG, Turtle CJ, et al. Chimeric antigen receptor-modified T cells derived from defined CD8+ and CD4+ subsets confer superior antitumor reactivity in vivo. Leukemia. 2016; 30:492–500. [PubMed: 26369987]
19. Berger C, Jensen MC, Lansdorp PM, Gough M, Elliott C, Riddell SR. Adoptive transfer of effector CD8+ T cells derived from central memory cells establishes persistent T cell memory in primates. The Journal of Clinical Investigation. 2008; 118:294–305. [PubMed: 18060041]
20. Berger C, Sommermeyer D, Hudecek M, Berger M, Balakrishnan a, Paszkiewicz PJ, et al. Safety of Targeting ROR1 in Primates with Chimeric Antigen Receptor-Modified T Cells. Cancer Immunology Research. 2014; 3:206–16. [PubMed: 25355068]
21. Macchia I, Gauduin M-C, Kaur A, Johnson RP. Expression of CD8α identifies a distinct subset of effector memory CD4+ T lymphocytes. Immunology. 2006; 119:232–42. [PubMed: 16836648]
22. Lee DW, Kochenderfer JN, Stetler-Stevenson M, Cui YK, Delbrook C, Feldman SA, et al. T cells expressing CD19 chimeric antigen receptors for acute lymphoblastic leukaemia in children and young adults: a phase 1 dose-escalation trial. The Lancet. 385:517–28.
23. Engelhardt B. Molecular mechanisms involved in T cell migration across the blood-brain barrier. J Neural Transm (Vienna). 2006; 113:477–85. [PubMed: 16550326]
24. Kranick S, Phan G, Kochenderfer J, Rosenberg S, Nath A. Aphasia As a Complication Of CD19-Targeted Chimeric Antigen Receptor Immunotherapy (S52.006). Neurology [Internet]. 2014; 82 Available from: http://www.neurology.org/content/82/10_Supplement/S52.006.abstract.
25. Reagan PM, Friedberg JW. Reassessment of Anti-CD20 Therapy in Lymphoid Malignancies: Impact, Limitations, and New Directions. Oncology (Williston Park). 2017; 31:402–11. [PubMed: 28516439]
26. Louveau A, Smirnov I, Keyes TJ, Eccles JD, Rouhani SJ, Peske JD, et al. Structural and functional features of central nervous system lymphatic vessels. Nature. 2015; 523:337–41. [PubMed: 26030524]
27. Bakken TE, Miller JA, Ding S-L, Sunkin SM, Smith KA, Ng L, et al. A comprehensive transcriptional map of primate brain development. Nature. 2016; 535:367–75. [PubMed: 27409810]
28. Tian L, Ma L, Kaarela T, Li Z. Neuroimmune crosstalk in the central nervous system and its significance for neurological diseases. Journal of Neuroinflammation. 2012; 9:155. [PubMed: 22747919]
29. da Fonseca ACC, Matias D, Garcia C, Amaral R, Geraldo LH, Freitas C, et al. The impact of microglial activation on blood-brain barrier in brain diseases. Frontiers in Cellular Neuroscience. 2014; 8:362. [PubMed: 25404894]

30. Romme Christensen J, Börnsen L, Hesse D, Krakauer M, Sørensen PS, Søndergaard HB, et al. Cellular sources of dysregulated cytokines in relapsing-remitting multiple sclerosis. Journal of Neuroinflammation. 2012; 9:215. [PubMed: 22978757]

31. Fragoso-Loyo H, Richaud-Patin Y, Orozco-Narvaez A, Davila-Maldonado L, Atisha-Fregoso Y, Llorente L, et al. Interleukin-6 and chemokines in the neuropsychiatric manifestations of systemic lupus erythematosus. Arthritis Rheum. 2007; 56:1242–50. [PubMed: 17393453]

32. Dutcher JP, Schwartzentruber DJ, Kaufman HL, Agarwala SS, Tarhini AA, Lowder JN, et al. High dose interleukin-2 (Aldesleukin) - expert consensus on best management practices-2014. Journal for ImmunoTherapy of Cancer. 2014; 2:26.

33. Kessing CF, Tyor WR. Interferon-α Induces Neurotoxicity Through Activation of the Type I Receptor and the GluN2A Subunit of the NMDA Receptor. Journal of Interferon & Cytokine Research. 2015; 35:317–24. [PubMed: 25517826]

34. Topp MS, Gokbuget N, Stein AS, Zugmaier G, O'Brien S, Bargou RC, et al. Safety and activity of blinatumomab for adult patients with relapsed or refractory B-precursor acute lymphoblastic leukaemia: a multicentre, single-arm, phase 2 study. Lancet Oncol. 2015; 16:57–66. [PubMed: 25524800]

35. Gofton TE, Young GB. Sepsis-associated encephalopathy. Nat Rev Neurol. 2012; 8:557–66. [PubMed: 22986430]

36. Wardill HR, Mander KA, Van Sebille YZA, Gibson RJ, Logan RM, Bowen JM, et al. Cytokine-mediated blood brain barrier disruption as a conduit for cancer/chemotherapy-associated neurotoxicity and cognitive dysfunction. Int J Cancer. 2016; 139:2635–45. [PubMed: 27367824]

37. Hudecek M, Sommermeyer D, Kosasih PL, Silva-Benedict A, Liu L, Rader C, et al. The nonsignaling extracellular spacer domain of chimeric antigen receptors is decisive for in vivo antitumor activity. Cancer Immunol Res. 2015; 3:125–35. [PubMed: 25212991]

38. Kaur A, Daniel MD, Hempel D, Lee-Parritz D, Hirsch MS, Johnson RP. Cytotoxic T-lymphocyte responses to cytomegalovirus in normal and simian immunodeficiency virus-infected rhesus macaques. J Virol. 1996; 70:7725–33. [PubMed: 8892893]

39. Terakura S, Yamamoto TN, Gardner RA, Turtle CJ, Jensen MC, Riddell SR. Generation of CD19-chimeric antigen receptor modified CD8(+) T cells derived from virus-specific central memory T cells. Blood. 2012; 119:72–82. [PubMed: 22031866]

40. Wang J, Jensen M, Lin Y, Sui X, Chen E, Lindgren CG, et al. Optimizing adoptive polyclonal T cell immunotherapy of lymphomas, using a chimeric T cell receptor possessing CD28 and CD137 costimulatory domains. Hum Gene Ther. 2007; 18:712–25. [PubMed: 17685852]

41. Pitcher CJ, Hagen SI, Walker JM, Lum R, Mitchell BL, Maino VC, et al. Development and Homeostasis of T Cell Memory in Rhesus Macaque. The Journal of Immunology. 2002; 168:29–43. [PubMed: 11751943]

Significance

We provide the first immunologically-relevant, non-human primate model of B-cell-directed CAR T cell therapy-mediated CRS and neurotoxicity. We demonstrate CAR and non-CAR T cell infiltration in the CSF and in the brain during neurotoxicity resulting in pan-encephalitis, accompanied by increased levels of pro-inflammatory cytokines in the CSF.

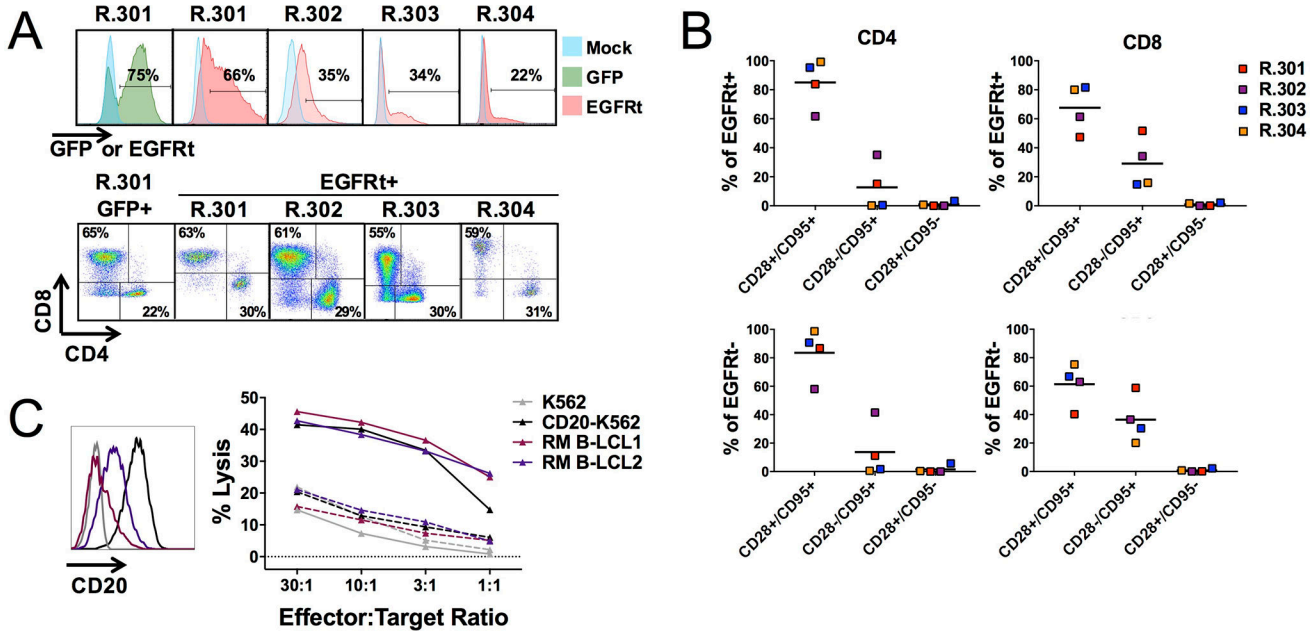

Figure. 1. RM GFP and CD20 CAR T cell product composition and function

A, GFP and EGFRt expression in RM T cell products transduced with GFP (R.301 GFP, green) or CD20 CAR (R.301–R.304 EGFRt, red); Mock (blue). CD8 and CD4 composition in RM GFP+ (R.301 GFP+) or EGFRt+ T cell products (R.301–R.304 EGFRt+). **B,** Composition of T cells in CD20 CAR products in EGFRt+ (top) and EGFRt− (bottom) CD4 and CD8 cells (R.301–R.304, $n = 4$). CD28+/CD95+: central memory, CD28−/CD95+: effector memory and CD28+/CD95−: naive T cells. Horizontal lines represent the mean. **C,** CD20 antigen expression in human (K562 and CD20-K562), and in RM (B-LCL1 and B-LCL2) cell lines. Cytolytic activity of RM mock-transduced (dashed lines) and CD20 CAR T cells (solid lines) against ^{51}Cr-labeled targets (K562, CD20-K562, B-LCL1 and B-LCL2). $n = 3$ replicates per point; representative of four recipients.

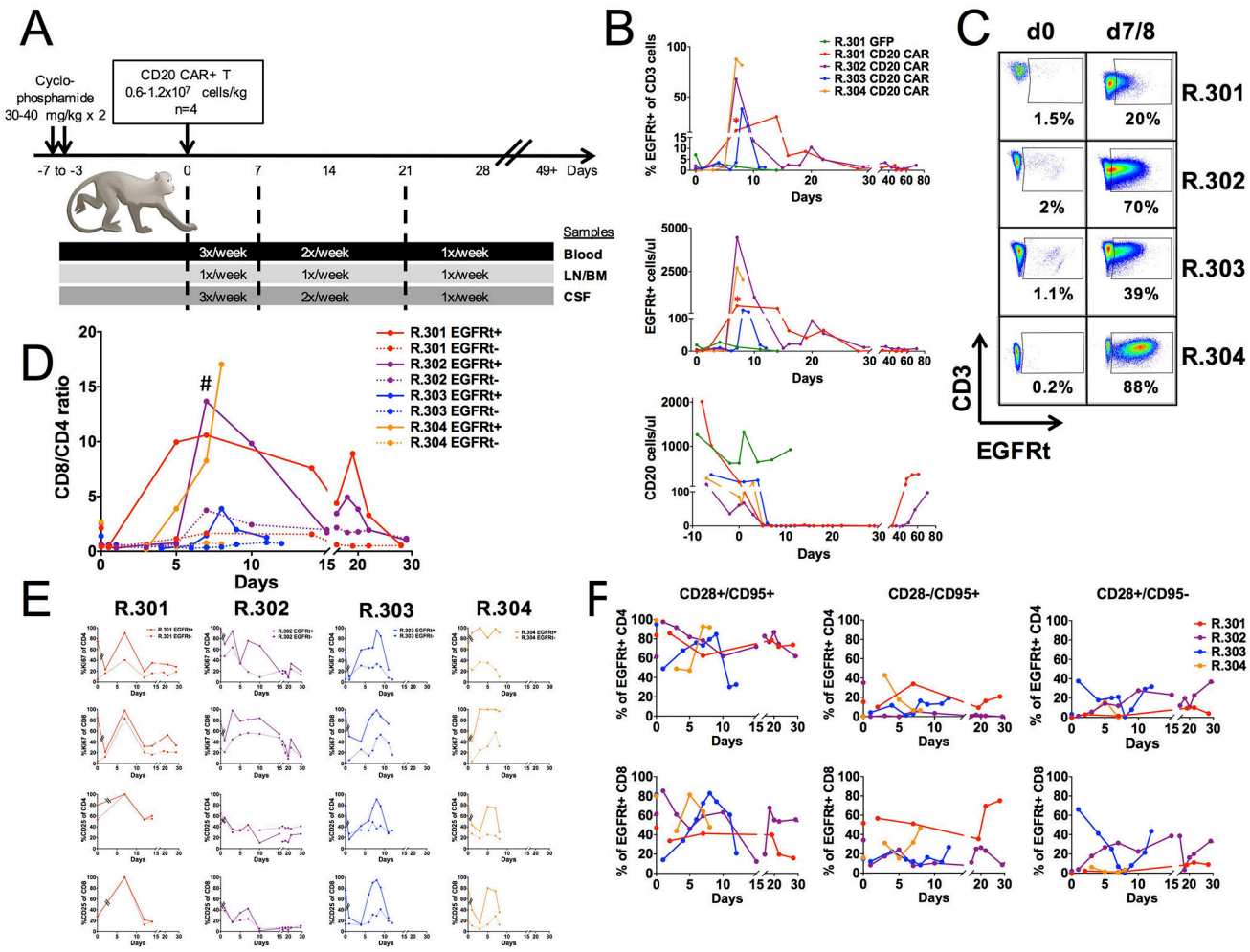

Figure 2. Adoptive transfer of RM GFP and CD20 CAR T cells and their dynamics *in vivo*

A, Animal schema for CD20 CAR RM studies with sample collection frequency. **B,** Percent (top) and absolute numbers (middle) of RM GFP+ or EGFRt+ (CD20 CAR) T cells and absolute number of CD20 cells (bottom) before and at indicated days after adoptive transfer in the blood. * denotes frozen PBMCs for day 7, R.301, CD20 CAR analysis. **C,** Frequency (%) of EGFRt+ cells of CD3+ T cells on day 0 (d0, prior to adoptive transfer) and on day of peak expansion, day 7 (R.301, R.302 and R. 304) or day 8 (R.303; (d7/8)) after adoptive transfer in the blood. **D,** EGFRt+ (solid lines) and EGFRt− (dotted lines) CD8 and CD4 T cell dynamics in the blood, expressed as CD8/CD4 ratio. Peak expansion vs pre-infusion EGFRt+ CD8/CD ratio: # $P = 0.03$. Dots on day 0 represent infused product samples. **E,** EGFRt+ (solid lines) and EGFRt− (dotted lines), CD4 (top and third from top panels) and CD8 (second from top and bottom panels) T cell proliferation (Ki67; top two panels), and activation (CD25; bottom two panels) in the blood *in vivo*. Broken lines after day 0 are used to indicate that the measurements on day 0 represent infused products and subsequent samples represent blood samples. Peak expansion measurements for R.301, R.302 and R. 304 were obtained on day 7 and for R.303 on day 8. Data are mean +/− s.e.m. **F,** EGFRt+ CD4 (top) and CD8 (bottom) T cell subset dynamics in the blood *in vivo*, represented by

CD28+/CD95+ (central memory), CD28−/CD95+ (effector memory) and CD28+/CD95− (naive). Dots on day 0 represent infused products.

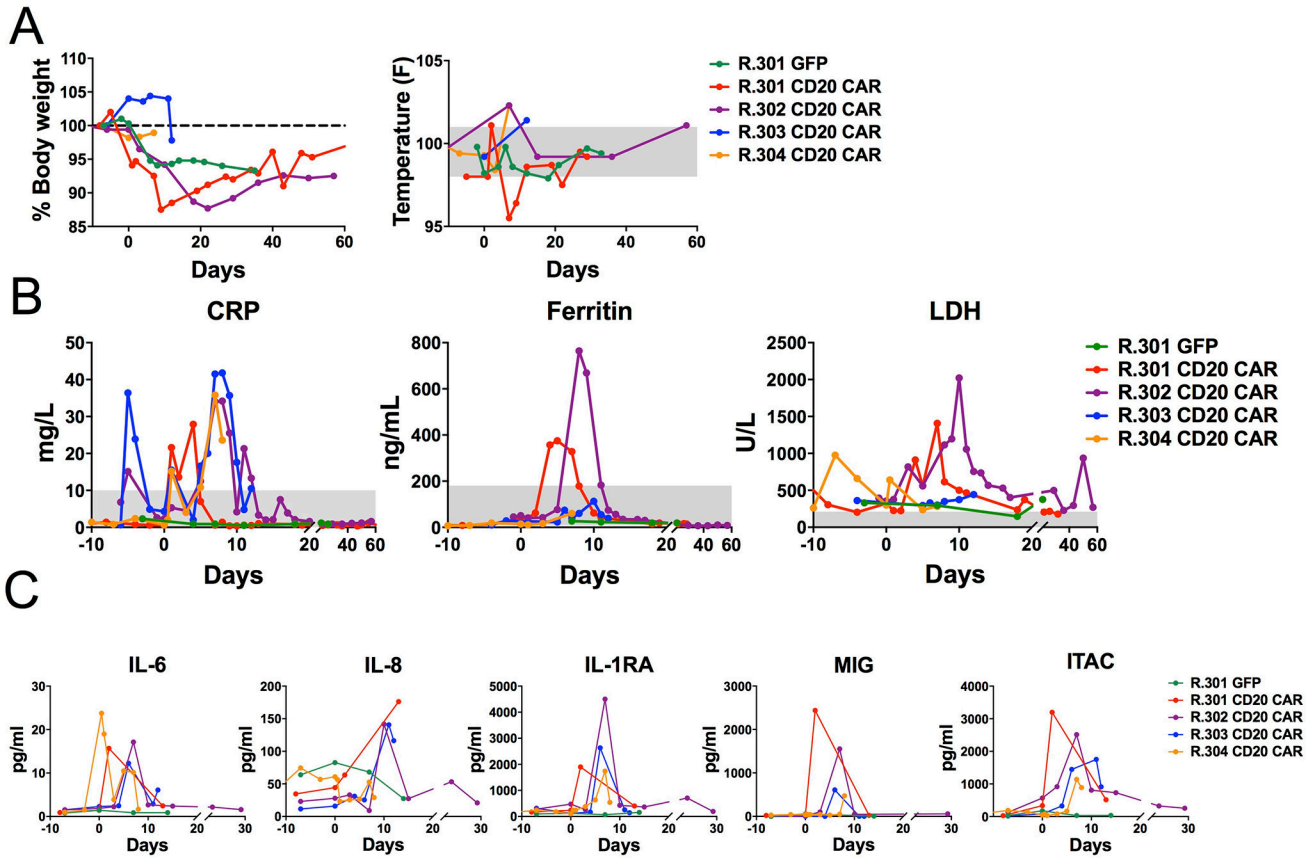

Figure 3. Clinical and biochemical markers of cytokine release syndrome (CRS) following adoptive transfer of RM CD20 CAR T cells

A, Changes in body weight and temperature (right). Normal temperature range shaded in gray. **B,** CRP, Ferritin and LDH levels before and at indicated days after GFP or CD20 CAR T cell transfer. Normal ranges are shaded in gray. **C,** Serum cytokine levels of IL-6, IL-8, IL-1RA, MIG and ITAC before and at indicated days after GFP or CD20 CAR T cell transfer.

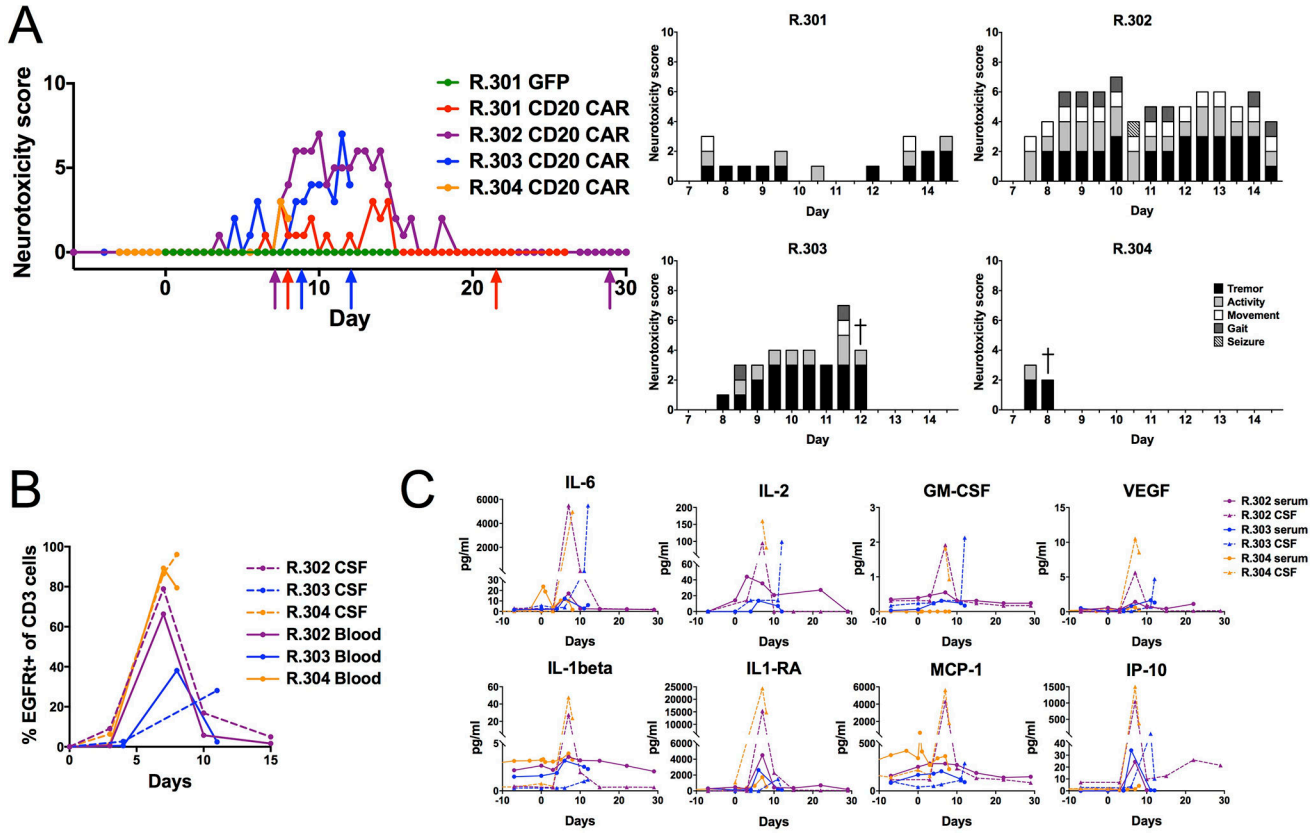

Figure 4. Neurologic toxicity is accompanied by increased T cell infiltration and disproportionately elevated cytokine levels in the CSF following adoptive transfer of RM CD20 CAR T cells

A, Neurotoxicity scores before and at indicated days after GFP or CD20 CAR T cell transfer. Arrows indicate the start and finish of Levetiracetam treatment (red:R.301, violet:R.302, blue:R.303). Neurologic symptoms contributing to the neurotoxicity score in R.301–R.304. **B,** Frequency (%) of EGFRt+ (CD20 CAR) T cells of CD3+ cells in the CSF (dashed lines) and in the blood (solid lines) following CD20 CAR T cell transfer in R.302–R.304. **C,** IL-6, IL-2, GM-CSF, VEGF, IL-1beta, IL1-RA, MCP-1 and IP-10 CSF (dashed lines) and serum levels (solid lines) before and at indicated days after CD20 CAR T cell transfer (R.302–R.304, $n = 3$).

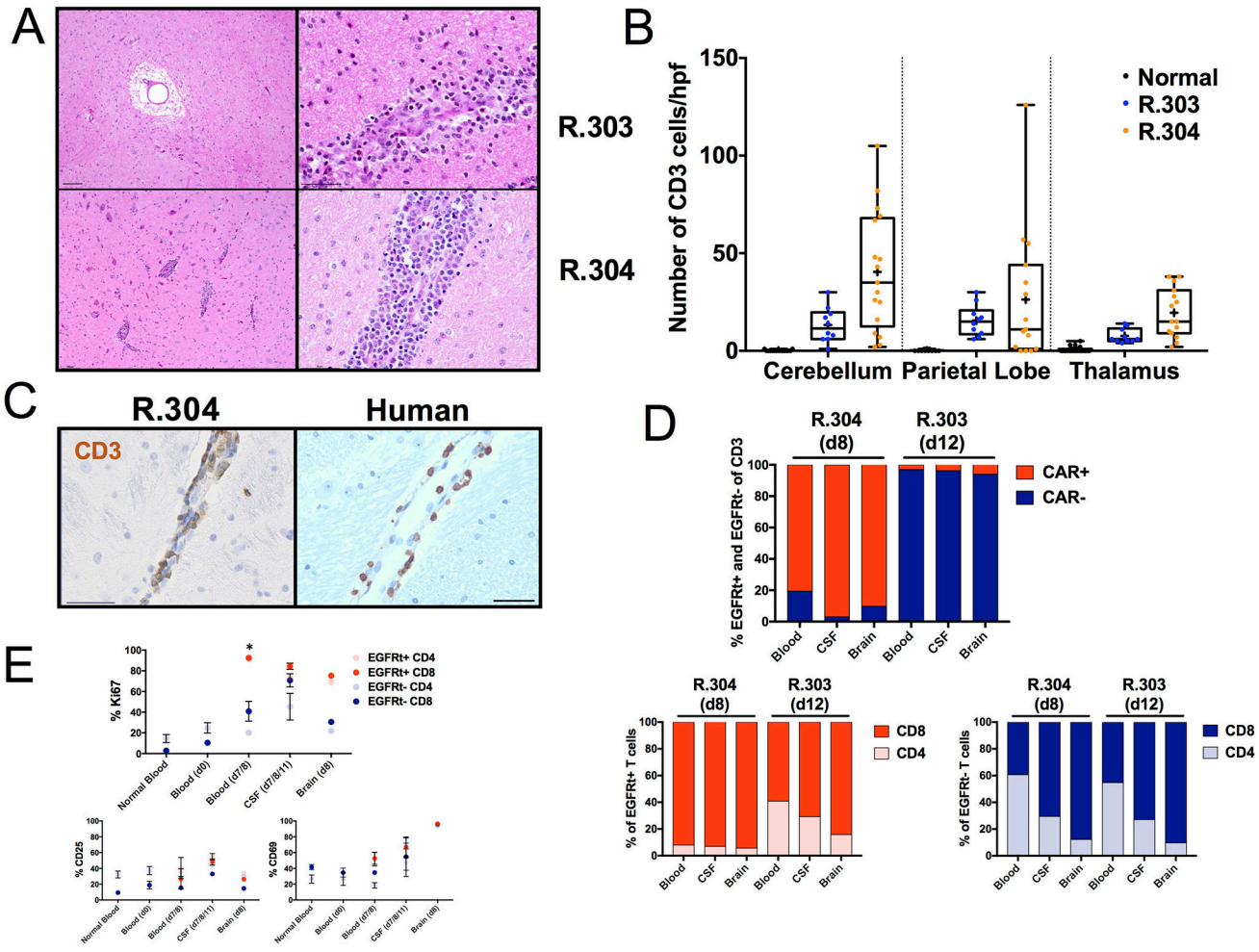

Fig 5. Perivascular T cells and infiltrative encephalitis by EGFRt+ (CD20 CAR) and EGFRt− (non-CAR) T cells following adoptive transfer of RM CD20 CAR T cells

A, H&E brain sections show focal perivascular edema (top left) and focal perivascular inflammation (top right) in R.303 and multifocal perivascular infiltration in the basal ganglia (bottom left) and parietal lobe (bottom right) in H&E sections in R.304. Scale bars, left: 100 μm; right: 50 μm). **B,** Enumeration of CD3+ T cell infiltration (quantified in 10–15 fields/brain region section at 20× magnification) in the cerebellum, parietal lobe and thalamus in normal RM, in R.303 (blue) and in R.304 (orange). Individual dots represent the number of CD3+ T cells per high power field. Box and whiskers represent the minimum and maximum range, 25th and 75th percentiles and the median range for all quantified fields in one section, + symbols indicate the mean. **C,** Cerebral perivascular CD3+ T cell infiltration in RM (R. 304) and in human brain of a patient with neurotoxicity after CD19 CAR T cell therapy. Scale bars: 50 μm. **D,** Percent EGFRt+ (CD20 CAR, red) and EGFRt− (non-CAR, blue) T cells and CD8:CD4 proportions in EGFRt+ (bottom left) and EGFRt− (bottom right) compartments in the blood, CSF and brain on day 8 (d8, R.304) and day 12 (d12, R.303). **E,** Fraction (%) of EGFRt+ or EGFRt− CD4 an CD8 T cells expressing Ki-67, CD25 or CD69 in the blood of normal RM controls ($n = 5$), on day 0, pre-CD20 CAR infusion (d0, $n = 4$) and on day 7 or 8 (peak CD20 CAR expansion, (days 7–8, $n = 4$)), in the CSF (on day 7 (R.

302), day 11 (R.303) and day 8 (R.304); days 7–8/11, $n = 3$) and in the brain (on day 8 (d8) in R.304, $n = 1$). * $P < 0.05$.